Applied Geochemistry 61 (2015) 272–283

Contents lists available at ScienceDirect

Applied Geochemistry

journal homepage: www.elsevier.com/locate/apgeochem

Kinetics of CO_2–fluid–rock reactions in a basalt aquifer, Soda Springs, Idaho

Alexandra Maskell [a,*], Niko Kampman [b], Hazel Chapman [a], Daniel J. Condon [c], Mike Bickle [a]

[a] Department of Earth Sciences, University of Cambridge, Downing Street, Cambridge CB2 3EQ, UK
[b] Shell Global Solutions International BV, Kesslerpark 1, 2288 GS Rijswijk, The Netherlands
[c] NERC National Isotope Geoscience Laboratories, Kinglsey Dunham Centre, Keyworth, Nottingham NG12 5GG, UK

ARTICLE INFO

Article history:
Received 16 September 2014
Revised 17 June 2015
Accepted 23 June 2015
Available online 24 June 2015
Editorial handling by M. Kersten

Keywords:
Carbon sequestration
CO_2–water–rock interaction
Feldspar dissolution
Gibbs free energy
Blackfoot Volcanic Field
Soda Springs

ABSTRACT

The dissolution of silicate minerals by CO_2-rich fluids and the subsequent precipitation of CO_2 as carbonate minerals represent a means of permanently storing anthropogenic CO_2 waste products in a solid and secure form. Modelling the progression of these reactions is hindered by our poor understanding of the rates of mineral dissolution–precipitation reactions and mineral surface properties in natural systems. This study evaluates the chemical evolution of groundwater flowing through a basalt aquifer, which forms part of the leaking CO_2-charged system of the Blackfoot Volcanic Field in south-eastern Idaho, USA. Reaction progress is modelled using changes in groundwater chemistry by inverse mass balance techniques. The CO_2-promoted fluid–mineral reactions include the dissolution of primary plagioclase, orthoclase, pyroxene and gypsum which is balanced by the precipitation of secondary albite, calcite, zeolite, kaolinite and silica. Mineral mole transfers and groundwater flow rates estimated from hydraulic head data are used to determine the kinetics of plagioclase and orthoclase feldspar dissolution. Plagioclase surface area measurements were determined using the evolution of the U-series isotope ratios in the groundwater and are compared to published surface area measurements. Calculated rates of dissolution for plagioclase range from 2.4×10^{-12} to 4.6×10^{-16} mol/m^2/s and orthoclase from 2.0×10^{-13} to 6.8×10^{-16} mol/m^2/s respectively. These feldspar reaction rates, correlate with the degree of mineral–fluid disequilibrium and are similar to the dissolution rates for these mineral measured in other natural CO_2-charged groundwater systems.

1. Introduction

Capture of carbon dioxide (CO_2) and subsequent storage in geological formations is widely seen as an important method for mitigating the effects of fossil fuel burning on global climate change (e.g. Intergovernmental Panel on Climate Change, 2013). Injection of CO_2 into basaltic aquifers is attractive due to the higher reactivity of mafic rocks compared to sandstone reservoirs, which may accelerate the conversion of injected CO_2 into solid phases (e.g. Kelemen and Matter, 2008; Kelemen et al., 2011; Matter and Kelemen, 2009). One of the outstanding scientific questions regarding injection of CO_2 in basaltic formations relates to the exact nature and rate of the subsequent CO_2-promoted mineral dissolution and precipitation reactions. Knowledge of the rates of these reactions is essential for accurate modelling of the long term fate of the injected CO_2.

Studies attempting to model the long term fluid–rock reactions in CO_2 storage sites typically use mineral reaction rate laws derived from laboratory experiments. However, there is a well-documented discrepancy of several orders of magnitude between the rates of silicate mineral dissolution derived from laboratory experiments and those derived from measurements in natural systems under comparable conditions of temperature and pH. These discrepancies may be due to the proximity of natural systems to equilibrium, ageing of mineral surfaces, difficulties associated with defining reactive mineral surface areas and the role of fluid transport processes as a rate limiting step in natural systems (e.g. Hellmann and Tisserand, 2006; Kampman et al., 2009; Maher, 2010; Maher et al., 2009; White and Brantley, 2003; Wigley et al., 2012). Further measurements of mineral reaction rates from natural systems are therefore required to constrain the controls of mineral fluid-kinetics in natural systems and to provide rate constants for use in fluid–rock reaction modelling.

In this study we model the nature and kinetics of mineral–fluid reactions which control fluid chemistry along groundwater flow

* Corresponding author.
E-mail address: am2031@cam.ac.uk (A. Maskell).

http://dx.doi.org/10.1016/j.apgeochem.2015.06.010
0883-2927/

paths in Soda Springs Valley Aquifer. Fluid–mineral reaction rates are constrained using (i) measured fluid and mineral chemistries, (ii) mineral surface area data and (iii) groundwater flow rates calculated from hydraulic head data and in-situ fracture permeability estimated from hydraulic well test data. Reactive mineral surface areas are estimated from mineral and fluid U-series isotope data and from geometric estimates using fracture surface area and mineral modal abundance data. The changes in groundwater chemistry along defined flow paths are modelled using mass balance of mineral dissolution and precipitation reactions and rates are derived using flow rate and mineral surface area data.

2. Geology

The Blackfoot Volcanic Field is located in southeastern Idaho along a transition zone between the Sevier Thrust Belt and the Basin and Range Province (Allmendinger, 1981; Hutsinpiller and Parry, 1985; Fig. 1). The major structures in the region are related to two major events, east–west compression during late Mesozoic to Eocene Sevier Orogen followed by Cenozoic basin and range extension with the formation of north–northwest-trending grabens and half-grabens (Allmendinger and Jordan, 1981; Armstrong and Oriel, 1965; Burchfiel et al., 1992; Camilleri et al., 1997). Extensive deposition of the fluvial Salt Lake Formation unconformably above Proterozoic and Palaeozoic rocks characterise this extensional period (e.g. Miller, 1991; Oriel, 1968; Oriel and Platt, 1980; Sacks and Platt, 1985). Several generations of faults cut the Salt Lake Formation indicating extension continued during the Late Miocene to Early Pliocene (Janecke and Evans, 1999). The Pleistocene marks a period of widespread volcanism in the region with dozens of volcanic vents and cinder cones emplacing the Blackfoot Lava Field, which ranges from a few metres thick at the margins to more than 300 m in the central parts of the basin, with individual flows up to 12 m thick (Mabey and Oriel, 1970). The volcanism is contemporary with the Snake River Plain volcanism to the north (Armstrong et al., 1975; Hutsinpiller and Parry, 1985).

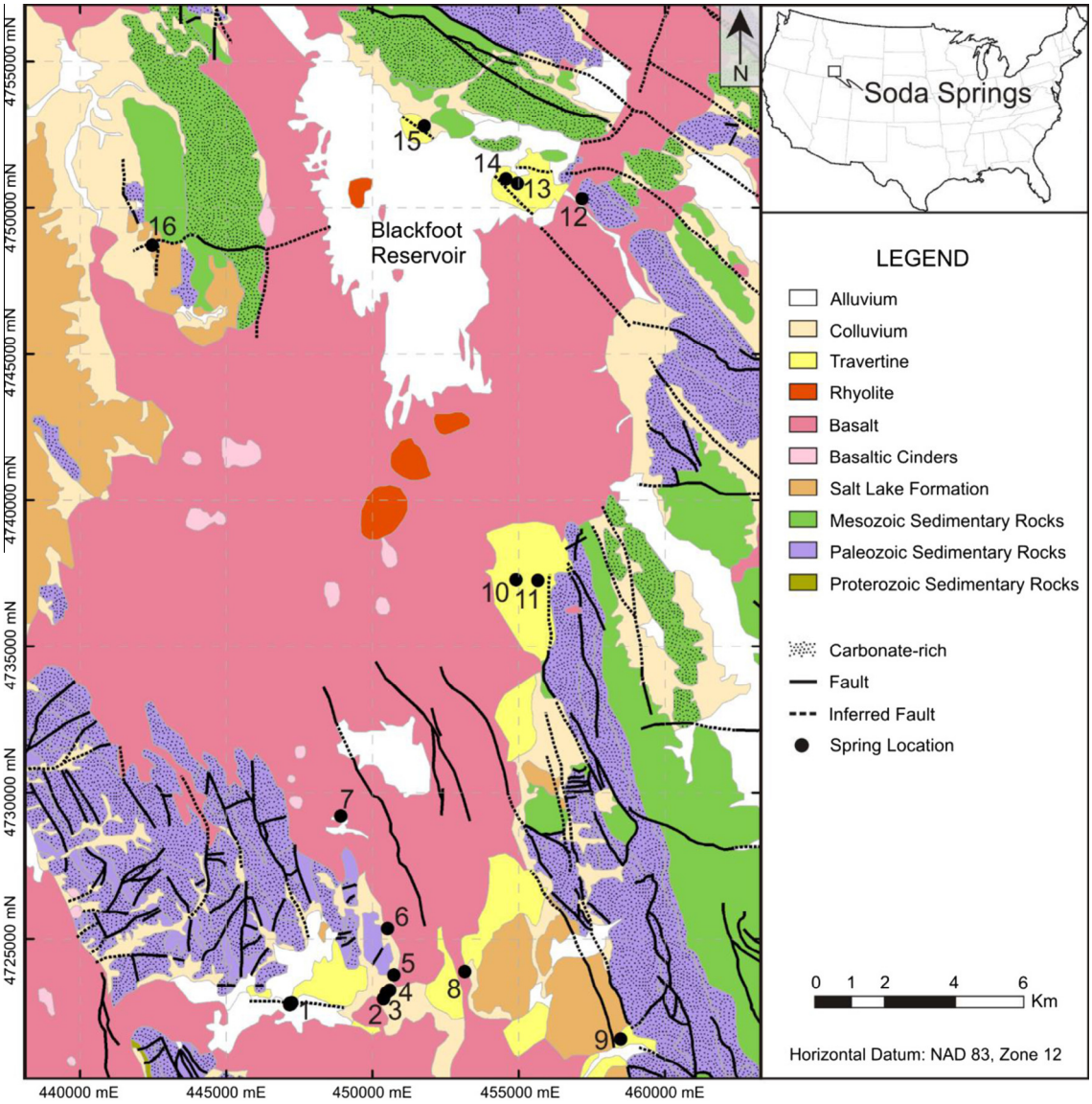

Fig. 1. Geological map of the Soda Springs-Blackfoot Reservoir region (Inset: Map of U.S.A. showing location of study area) after Mabey and Oriel (1970) showing geology and locations of springs. 1. Pavilion Well, Outhouse Spring, Thunderbox Spring, Dunny Spring; 2. Soda Geyser; 3. Hippie Spring; 4. Octagon Spring; 5. Lovers Delight Spring; 6. Hooper Spring; 7. Mammoth Spring; 8. Ledger Spring; 9. Sulphur Springs; 10. East Woodall Spring; 11. Sulphur Woodall Spring; 12. Little Blackfoot River Spring; 13. Warm Spring; 14. Henry Spring; 15. Lone Tree Spring; 16. Corral Creek Spring.

3. Hydrogeology and flow paths

Numerous thermal CO_2-rich springs, along with several artesian and abandoned geothermal exploration wells occur in the Blackfoot Volcanic Field (Hutsinpiller and Parry, 1985). These springs and wells issue from within or proximal to the margins of the basalt flows along north–northwest trending extensional faults. Small travertine deposits forming mounds and cones occur in direct association with the CO_2 springs. The close spatial association between extensional faults and springs suggest these faults act as conductive pathways for ascending groundwater. $CO_2/^3He$ and $\delta^{13}C$ ratios of selected CO_2-charged springs indicate that the CO_2 is derived from varying degree of crustal and mantle derived carbon (Jeandel et al., 2010). Recent work by Lewicki et al. (2013) mapped surface CO_2 fluxes and quantified the emissions of CO_2 around some of the springs.

The major sources of groundwater recharge in the region are upland precipitation and snowmelt around the edges of the basin, leakage from the Blackfoot Reservoir, seepage from streams and rivers along the margins of the basin, and possible underflow from the Bear River-Dingle Swamp groundwater system (Graham and Campbell, 1981). The hydrogeology of the Blackfoot Volcanic Field comprises two major groundwater regimes; an unconfined freshwater surficial aquifer in the upper basalt flows and scoria cones, and a multi-layered carbonate-rich aquifer semi-confined to the lower basalt flows and scoria cones. Hydraulic flow within the basalt travels preferentially along flow boundaries through rubble zones. Geochemical analyses of groundwater (Idaho Department of Water Resources, 2012) discharging from the upper freshwater aquifer indicates that there is mixing between the upper and lower groundwater regimes. On the basis that the upper aquifer and lower aquifers are in hydraulic communication, and as both portions of the aquifer are recharged in the regions surrounding the Blackfoot Volcanic, regional potentiometric surface maps are constructed from borehole data in wells penetrating the upper aquifer (Idaho Department of Water Resources, 2012). Flow paths and hydraulic head data for the lower aquifer are estimated from these maps. Groundwater flow is therefore considered to be predominately horizontal in both regimes, with a south to southwest flow direction that diverts to a westerly flow near Soda Springs. The sampled CO_2-charged springs discharge from faults and wells penetrating the lower aquifer and along a regional flow path (7-1; Fig. 1).

4. Sampling and analytical methods

4.1. Water sample collection

Water samples were collected from a total of 19 springs in the Blackfoot Lava Field during November 2011. All samples were filtered through 0.2 μm nylon filters on collection and stored in pre-cleaned, 3 M HCl and 18.2 MΩ deionized water washed polyethylene bottles, prewashed with filtrate. At least two samples were taken of each spring for major and trace element analysis, one being acidified with HNO_3 for cation analysis and one un-acidified for anion analysis. Eh, pH, temperature, and alkalinity (by Gran Titration; Stumm and Morgan, 1996) were measured in the field. The pH/Eh metre was calibrated daily on standard solutions of pH 4, 6 and 8.

4.2. Major and trace elements

Thirty water samples were analysed for Na, K, Ca, Mg, Si, Sr, Al, Ba, B, Fe, Mn, SO_4, Cl, and F at the University of Cambridge (Table S1). Cation analysis was conducted on acidified samples using a Varian Vista-Pro simultaneous Inductively Coupled Plasma Atomic Emission Spectrometer (ICP-AES) and anion analysis on un-acidified samples using a Dionex Ion Chromatography System. International river and lake water standards T-149, T-167, LGC 6019, SPS-SW2 were dispersed between samples to determine the accuracy of data. Standards gave concentrations within 3% of listed values.

Analysis of $^{87}Sr/^{86}Sr$ was conducted on twelve samples at the University of Cambridge. Strontium was separated using Dowex 50Wx8 cation exchange resin with 200–400 mesh particle size in ultra-clean lab conditions and $^{87}Sr/^{86}Sr$ ratios were measured on a VG Sector 54 solid source mass-spectrometer using triple-collector dynamic algorithm, normalised to $^{86}Sr/^{88}Sr$ 0.1194 with an exponential fractionation correction (cf. Bickle et al., 2003, 2005). The 52 analyses of NBS 987 during the two year period in which these samples were analysed gave a mean value of 0.710260 ± 8 ppm (1 sigma). A Sr blank measured at the same time as the samples was 65 pg, negligible compared with the >1 μg Sr separated for analysis.

U-series analysis was conducted on six samples at the British Geological Survey's Nottingham NERC Isotope Geosciences Laboratory using a Multi-collector Inductively Coupled Plasma Mass Spectrometer (MC-ICP-MS). Precision for $^{234}U/^{238}U$ is ±~3%. Element selective columns were used to pre-concentrate the uranium, to achieve maximum sensitivity, and eliminate matrix elements to enhance the accuracy and precision obtained.

δD and $\delta^{18}O$ isotopes were analysed in twenty samples at the Godwin Laboratory, University of Cambridge using a Thermo Finnigan stable isotope mass spectrometer. Analyses are expressed in δ ‰ deviation relative to VSMOW standards with analytical precisions estimated at ±1.0 and ±0.1‰ for δD and $\delta^{18}O$ respectively.

5. Discussion and results

5.1. Well test and bulk hydraulic conductivity

Groundwater principally moves through fractures and rubble zones in the basalt. The in-situ bulk hydraulic conductivity of the fractured basalt was estimated from pressure recovery data collected during flow testing of Pavilion Well, which discharges CO_2-charged fluid from the lower aquifer. Gas and water discharge were estimated using a venturi metre and by collection of the discharged water into a known volume. After discharging for approximately 5.5 h, a relatively constant flow rate was achieved. The well was then shut-in and pressure data was logged for the time it took to stabilise (Fig. 2a). The pressure gauge was monitored and data recorded in response to changes in pressure.

The Bisroy and Summers (1980) recovery method for analysing single-well tests with variable discharge rates in a confined aquifer was used to estimate the hydraulic conductivity. The residual drawdown response is determined analytically using Eq. (1) from Bisroy and Summers (1980). The slope of a semi-log plot of the residual drawdown (s') divided by constant discharge (Q) versus adjusted time (Fig. 2b), can be used to determine the transmissivity and hydraulic conductivity by:

$$slope = \Delta\left(\frac{s'}{Q_n}\right) = \frac{2.30}{4\pi KD} \quad (1)$$

This gave a bulk hydraulic conductivity of $1.2 \times 10^{-4} \pm 1.8 \times 10^{-5}$ m/min. Uncertainty was calculated using the equations in Appendix A. Drilling conducted by the U.S. Army Engineers (1968) in the upper aquifer on the southern edge of Blackfoot Reservoir gave a similar range of hydraulic conductivity values ranging from 3.05×10^{-6} to 6.71×10^{-4} m/min. The calculated value in this study (1.2×10^{-4} m/min) was taken to apply to whole aquifer.

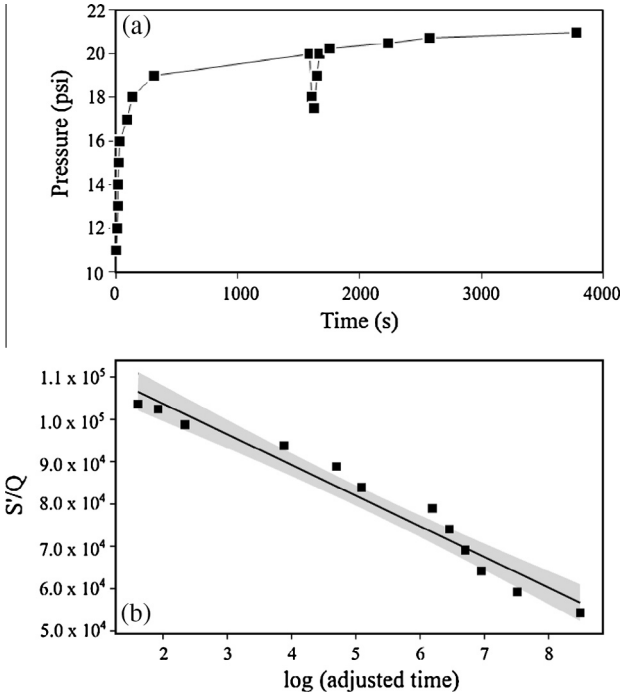

Fig. 2. (a) Build-up graph of pressure versus shut-in time: Pavilion well was left to flow for 5.5 h (approx. 2000 s) before the well was shut in and pressure data measured until the reservoir recovered. The pressure gauge was monitored and data recorded in response to changes in pressure. The sudden decrease in pressure at 1500 s is attributed to where increasing bottom-hole pressure becomes greater than the capillary pressure of the formation and water is forced back into the formation; (b) Semi-log plot of s'/Q versus log (adjusted time), see Bisroy and Summers (1980) for details on this analysis. Squares show measured values; the black line, fitted values; and the grey region is the error envelope of the fit.

5.2. Flow rate estimates

Flow rates, needed for the calculations of mineral reaction rates, have been calculated by parameterising the hydraulic head along the one dimensional flow path (springs 7-1; Fig. 1) with the approximation (Fig. 3):

$$h = a \cdot \exp(-bz) \quad (2)$$

where z is distance along flow (m) and the constants, a = 0.0288 and $b = 6.074 \times 10^4$, were determined by a least-squares fit.

The velocity in the groundwater system is then given by Darcy's Law:

$$v_a = -k \cdot (h)/\varphi = -0.0288 \cdot \exp(-6.074 \times 10^4 \cdot z)k/\varphi \quad (3)$$

where v_a is the real velocity (m/s), k is the bulk hydraulic conductivity (m^2), and φ is the porosity of the aquifer.

5.3. Flow path chemistry

Table 1 lists the surface temperatures, pH, Eh, and alkalinity present in water samples from along flow path. The chemical variation of groundwater over space and time is dependent on chemical and biologically-mediated reactions between groundwater and host rocks.

Concentrations of Ca, K, Mg, Sr, Al and SO_4 increase, and Na, B, Ba, Cl, F, Mn and SiO_2 decrease along the flow path (selected elements are shown in Fig. 4.; data available in Supplementary Material, Table S1). Alkalinity and pH increase along the flow path as a result of fluid rock reactions consuming H^+ and CO_2, producing HCO_3^-. The Sr/Ca ratio remains constant as both Ca and Sr concentrations increase along the flow path and the Ca/Sr ratio in the water is comparable to that of plagioclase feldspar in the host basalt (plagioclase composition is discussed further is Section 5.4.1.) consistent with the changes in the Ca and Sr concentrations being dominated by inputs from plagioclase dissolution.

Overall concentrations of chloride are low, indicating little or no input of basinal brines. SO_4 increases along the flow path, however, as Cl displays a decreasing trend the source of S is unlikely to be derived from the mixing of deeper formation brines from the underlying Salt Lake Formation. It is more likely that the increase is due to dissolution of gypsum/anhydride, as suggested by Lewicki et al. (2013). The groundwater becomes progressively more reduced along the flow path. The δD and $\delta^{18}O$ compositions of the springs in the Soda Springs basalt aquifer define a linear array which overlaps the Local Meteoric Water Line defined for the wider region (LMWL; for south-eastern Idaho, western Wyoming and south-central Montana from Benjamin et al., 2004; Fig. 5).

The concentration and ratio of conservative tracers in the most upstream Mammoth Spring are similar to those measured in Blackfoot reservoir (Supplementary Material, Table S1), suggesting that groundwaters discharged from this spring are largely derived from the same recharge inputs as the reservoir. Further downstream conservative ion tracers (Cl, F, B) and δD and $\delta^{18}O$ ratios covary and change systematically to more dilute and isotopically light compositions. The decrease in conservative ion tracers could be a due to the gradual addition of meteoric water from along the flow path. The changes in δD and $\delta^{18}O$ ratios are attributed to the older waters in the downstream parts of the flow path reflecting changing climatic conditions. Fluid transit times along flow paths from zones of recharge in the north to discharge at Pavilion Well, are estimated to be approximate 19,000 years based on hydraulic head and conductivity measurements from this study. Thus the oldest waters were sourced during the last glacial maximum when local $\delta^{18}O$ and δD of local surface waters was substantially lighter (Bright et al., 2006; Jimènez-Moreno et al., 2007) and recharge waters were likely to be dominated by snow melt.

The marked decrease in pH at Lovers Delight spring and subsequent rapid increase is interpreted to indicate a fresh addition of CO_2 at this location, derived from local extensional faults. The rapid increase in the concentrations of Ca, Sr, K and SO_4 downstream of Lovers Delight is inferred to be the result of fluid–rock reactions driven by the addition of CO_2 coupled with the decreasing fluid velocities reflecting the decline in the gradients in hydraulic head (Fig. 6). The rate of change in fluid chemistry decreases with distance downstream of Lovers Delight spring.

5.3.1. Strontium isotopes

$^{87}Sr/^{86}Sr$ ratios of the groundwaters range from 0.70851 to 0.70915 (Fig. 7). In the first part of the flow path (Mammoth spring to Lovers Delight) $^{87}Sr/^{86}Sr$ ratios increase while Sr concentrations remain approximately constant interpreted to reflect mixing of water sources and/or exchange. Downstream of Lovers Delight spring Sr concentrations increase and $^{87}Sr/^{86}Sr$ ratios decrease towards ratios consistent with the addition of Sr derived from the host basalt, most likely dominated by the dissolution of plagioclase.

5.3.2. $^{234}U/^{238}U$ Isotope ratio

Several studies have used ^{238}U, ^{234}U and ^{222}Rn isotopes due to their relative solubility to constrain the source, age and the degree of mixing of ground waters (e.g. Osmond and Cowart, 1976; Osmond et al., 1983; Luo et al., 2000; Roback et al., 2001; Maher et al., 2004).

The spring $^{234}U/^{238}U$ activity ratios shown in Table 2, are elevated relative to the largest source of recharge water in the region, rainfall and snowmelt (which has a $^{234}U/^{238}U$ activity ratio of

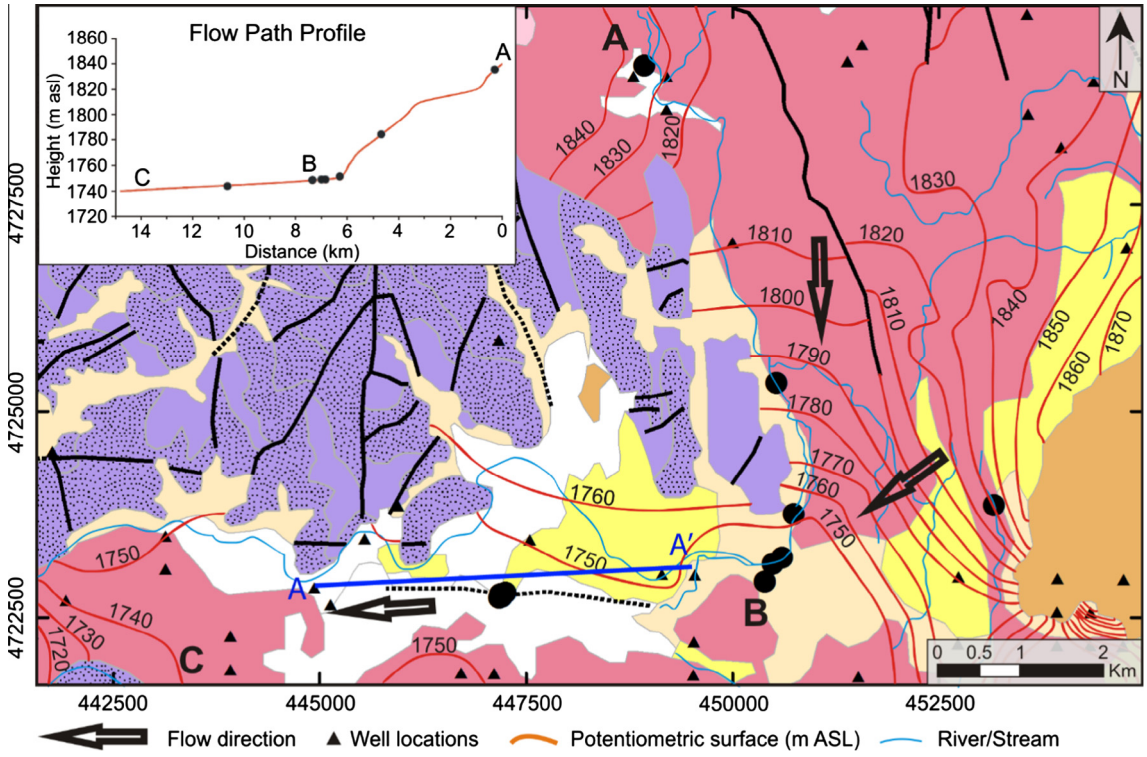

Fig. 3. Potentiometric map of upper aquifer overlaid over geology. Legend as for Fig. 1. Triangles indicate location of wells used in interpolation. The graph in the top left corner shows the potentiometric surface along the investigated flow path from A to B to C. The flow path profile is approximated by Eq. (2) to simplify later calculations of reaction rates.

Table 1
Data of sampled springs (sampled in Nov 2011). Discharge was estimated using the float method. Numbers in column 1 correlate with spring locations in Fig. 1.

Map Loc. Fig. 1	Name	Easting	Northing	Temp (°C)	pH	Eh (mV)	Field Alk. (mEq/l)	Discharge (L/s)
1	Pavilion Well	447253	4,722,798	26.9	6.31	−40	41.58	0.14
1	Dunny Spring	447,189	4,722,779	29.6	6.34	−68	41.62	–
1	Thunderbox Spring	447,176	4,722,735	28.8	6.35	−74	41.11	–
1	Outhouse Spring	447,208	4,722,747	29.1	6.27	−42	41.85	–
2	Soda Geyser	450,394	4,722,933	29.8	6.34	10	42.66	–
2	Soda Geyser (eruption)	450,394	4,722,933	25.3	6.60	8	41.94	~7570[a]
3	Hippy Spring	450,493	4,723,147	25.2	6.23	13	34.70	–
4	Lovers Delight	450,744	4,723,753	9.5	6.05	60	22.74	0.24
5	Octagon Spring	450,605	4,723,226	15.0	6.11	16	33.79	16.91
6	Hooper Spring	450,534	4,725,340	9.8	6.10	80	16.61	34.83
7	Mammoth Spring	448,934	4,729,188	11.7	5.90	74	19.05	194.62
8	Ledger Spring	453,172	4,723,864	9.7	7.22	204	9.35	–
9	Sulphur Springs	458,505	4,721,554	−0.2	5.97	−215	10.71	–
10	East Woodall	454,921	4,737,268	8.9	7.40	–	9.07	–
11	Sulphur Woodall	455,671	4,737,237	8.7	7.35	–	10.22	–
12	Little Blackfoot River	457,182	4,750,291	14.2	6.93	46	11.73	–
13	Warm Spring	454,575	4,750,981	22.0	6.33	13	15.57	–
14	Henry Spring	454,972	4,750,825	22.4	6.28	45	16.67	–
15	Lone Tree	451,785	4,752,791	21.3	6.46	40	17.81	3[b]
16	Coral Creek	442,478	4,748,705	17.0	6.34	80	45.41	–

[a] Mitchell (1976).
[b] Ralston et al. (1983).

~1.05; Martínez-Aguirre et al., 1991). The increase in $^{234}U/^{238}U$ activity ratios along flow path is interpreted to result from addition of ^{234}U due to alpha-recoil processes close to mineral surfaces.

5.4. Reaction progression

The evolution of chemical concentrations and isotopic ratios are used to constrain mass balance models of fluid–rock reactions. For the calculation of mineral reactions only the 4 springs downstream of Lovers Delight spring are used, where the spatial changes are well constrained and thought not to be the result of mixing of different fluids. Mineral dissolution rates can then be calculated from the chemical evolution of these groundwaters along the flow path, using estimates of mineral surface areas and fluid velocities determined from gradients in hydraulic head data and the measured in-situ permeability measurement.

The saturation states of the spring waters were calculated using the geochemical modelling software PHREEQC (Parkhurst and Appelo, 1999) coupled with the llnl.dat thermodynamic database (Johnson et al., 2000). The calculations show that the waters are

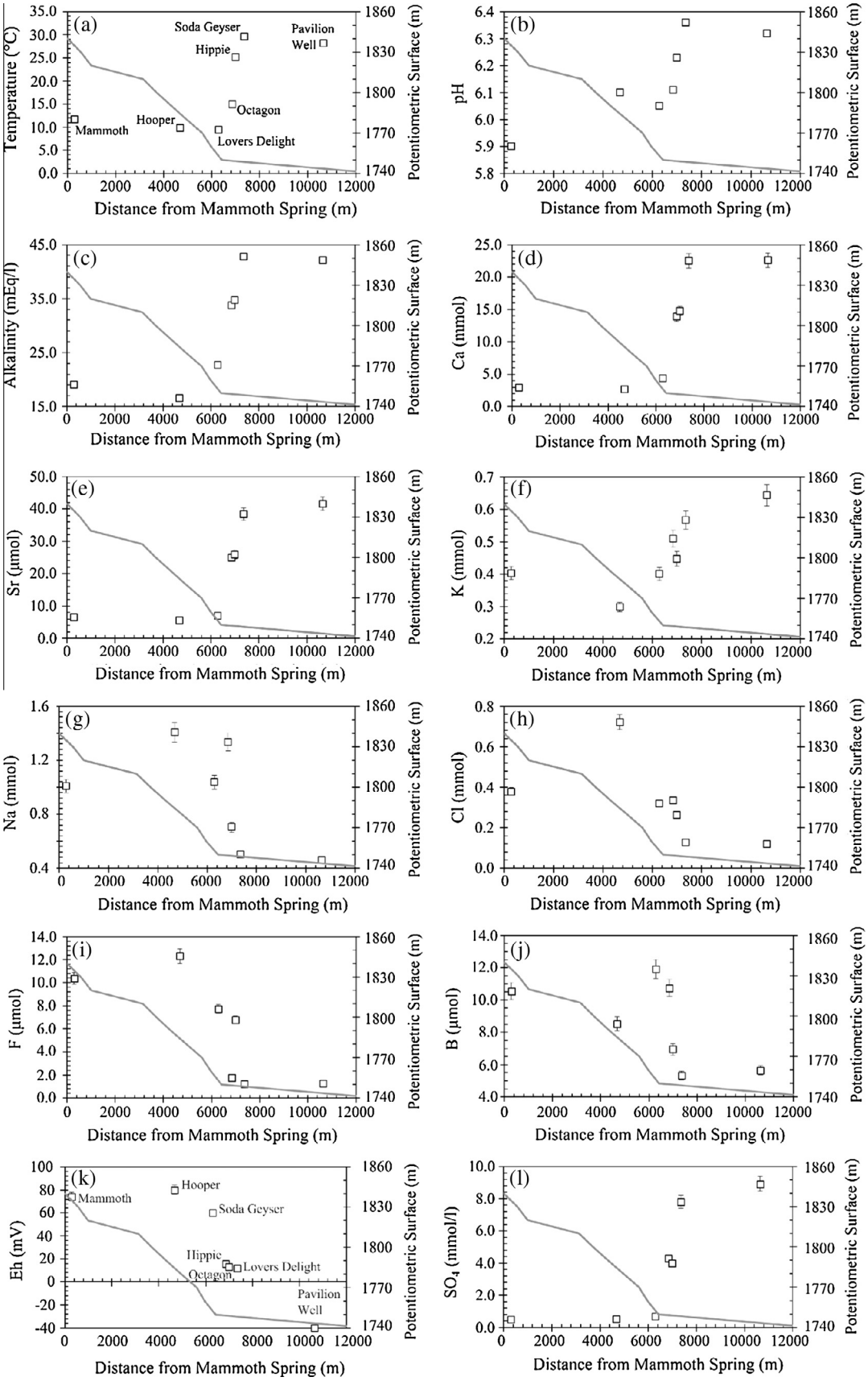

Fig. 4. Plots showing the changes in temperature, pH and solute concentrations with distance along the flow path. Line shows potentiometric heights (right hand axis). Vertical error bars show analytical error, where not visible the error is smaller than the symbol.

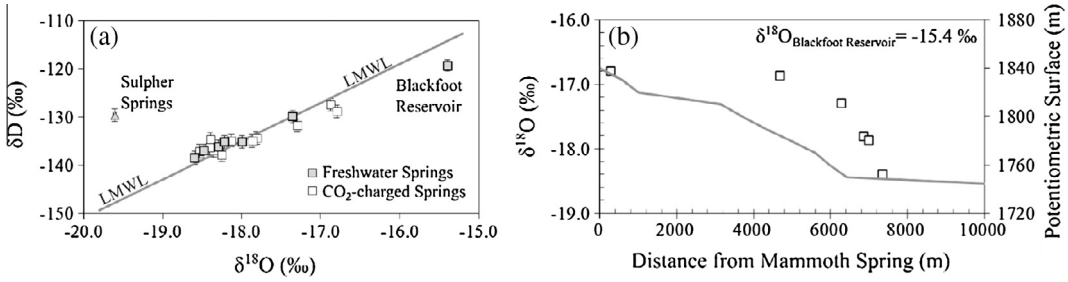

Fig. 5. Geochemical plots of (a) δD against $\delta^{18}O$, showing the meteoric water line for south-eastern Idaho, western Wyoming and south-central Montana (Benjamin et al., 2004) (b) $\delta^{18}O$ against distance along flow path. Line shows potentiometric heights (right hand axis).

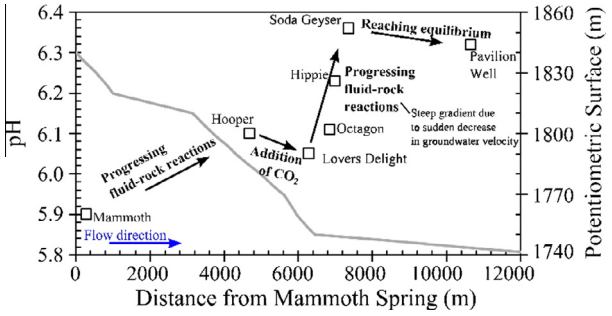

Fig. 6. Annotated plot of pH versus distance from Mammoth spring along the flow path. From Mammoth spring to Hooper spring fluid–rock reactions progress, at Lovers Delight spring a decrease in pH of 0.15 units is interpreted to indicate fluid mixing with the addition of a CO_2-rich fluid. The subsequent increase in pH from Lovers Delight spring to Soda Geyser along with an increase in the contributions of solutes from fluid–rock reactions, i.e. plagioclase and pyroxene dissolution, suggests continuing fluid–rock reactions. The sharp gradient is due to the slowing of groundwater allowing a longer residence time for reactions to take place. Continuing along the flow path, by time it reaches Pavilion well, the groundwater is nearing equilibrium.

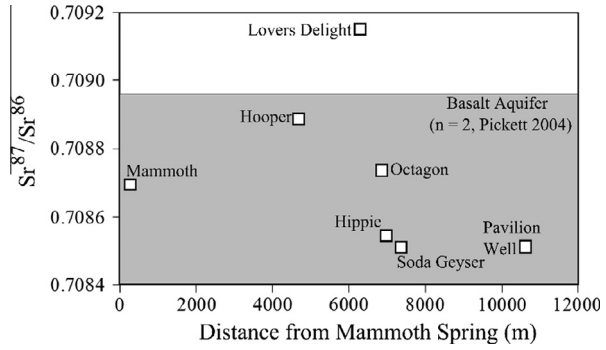

Fig. 7. Plot of $^{87}Sr/^{86}Sr$ ratios versus distance along flow path, the grey region shows the range of $^{87}Sr/^{86}Sr$ ratios of the host basalt (taken from Pickett, 2004). The sharp increase in Sr isotopic ratio at Lovers Delight Spring (~5 km) is indicative of groundwater mixing with a more radiogenic fluid. The subsequent decrease in $^{87}Sr/^{86}Sr$ ratios coincides with a sharp increase in Sr and Ca concentrations, with a Sr/Ca ratio of the host rock plagioclase (Fiesinger et al., 1982).

under-saturated in possible primary mineral phases (Na–Ca plagioclase, olivine, Mg–Fe clinopyroxene, orthoclase) and oversaturated in likely secondary reaction products (calcite, chalcedony, kaolinite, mesolite). Albite, scolecite and CO_2 (g) vary between under-saturated and saturated states along the flow path.

5.4.1. Mass balance calculations

The change in the dissolved chemical component Δm_k in groundwater due to mineral dissolution–precipitation reactions is given (Drever, 1988) as:

$$\Delta m_k = \sum_{j=1} M_j b_{j,k} \quad (4)$$

Table 2
$^{234}U/^{238}U$ activity ratios of spring samples. Hippie spring was not analysed.

Spring	Spring Name	$^{234}U/^{238}U$
7	Mammoth Spring	1.80
6	Hooper Spring	1.92
5	Lovers Delight	1.71
4	Octagon Spring	1.78
3	Hippie spring	–
2	Soda Geyser #2	2.83
1	Pavilion Well	7.44

where M_j is the number of mols of mineral j transferred to the fluid (negative for precipitation) and $b_{j,k}$ is the stoichiometric mol fraction of chemical constituent k in mineral j. The following mineral compositions, as determined from electron probe analyses and published whole rock geochemical data by Pickett (2004) and Fiesinger et al. (1982), were used to constrain the mass balance model:

Plagioclase: $Ca_{0.5}Na_{0.5}Al_{1.5}Si_{2.5}O_8$[a].
Orthoclase: $KAlSi_3O_8$[b].
Albite: $NaAlSi_3O_8$[b].
Pyroxene: $(Mg_{0.4}Ca_{0.3}Fe_{0.3})_2Si_2O_6$[a].
Gypsum: $CaSO_4{\cdot}2H_2O$[b].
Kaolinite: $Al_2Si_2O_5(OH)_4$[b].
Zeolite: $Na_2Al_2Si_3O_{10}{\cdot}3H_2O$–$Ca_2Al_2Si_3O_{10}{\cdot}3H_2O$[c].
Calcite: $CaCO_3$[b].
Quartz: SiO_2[b].

([a]Electron Probe, [b]ideal composition, [c]solid solution with two end-members treated independently).

The net transfer of major minerals to the fluid was calculated from the evolution of spring chemistry between the most upstream spring not affected by fluid mixing, Lovers Delight Spring, and all successive down-flow springs.

The following mass transfer reactions between groundwater and the basalt aquifer were constrained by the above mineral compositions and the changes in eight chemical components (Al, Ca, K, Mg, Na, SO_4, Si and Sr) along the flow path, whereby reactions comprise: (1) the dissolution of plagioclase, orthoclase, pyroxene and gypsum, (2) the precipitation of calcite, zeolites, albite, silica and kaolinite. Zeolite precipitation was assumed to account for excess Ca, Na and Si.

$$\Delta m_{T,Ca} = 0.5M_{plagioclase} + 0.3M_{pyroxene} + M_{gypsum} + M_{calcite} + (0.32{-}.336)M_{zeolite} \quad (5)$$

$$\Delta m_{T,K} = M_{orthoclase} \quad (6)$$

$$\Delta m_{T,Na} = 0.5M_{plagioclase} + M_{albite} + (0.278{-}0.368)M_{zeolite} \quad (7)$$

$$\Delta m_{T,Mg} = 0.4M_{pyroxene} \quad (8)$$

$$\Delta m_{T,Al} = M_{plagioclase} + M_{orthoclase} + 2M_{zeolite} \quad (9)$$

$$\Delta m_{T,Si} = 3M_{plagioclase} + 2M_{pyroxene} + 3M_{orthoclase} + 3M_{albite} + M_{silica} + 3M_{zeolite} \quad (10)$$

$$\Delta m_{T,S} = M_{gypsum} \quad (11)$$

Plagioclase, clinopyroxene, orthopyroxene and orthoclase have known Sr partition coefficients of 2.7, 0.157, 0.0068 and ~3 respectively (White, 2011). Consequently Sr is highly compatible in the feldspars. As the Sr/Ca ratio added to the groundwater (0.0018) is equal to the plagioclase Sr/Ca ratio of 0.00188 ($2\sigma = 0.000292$, $n = 11$) it can be inferred that plagioclase hosts 'all' the Sr and thus Sr can be used as a proxy to determine plagioclase mole transfers. Using $^{87}Sr/^{86}Sr$ isotopes and Sr concentrations the following mass balance equations can be derived:

$$\Delta Sr = Sr_{final} - Sr_{initial} \tag{12}$$

$$\Delta^{87}Sr/^{86}Sr \cdot Sr = (^{87}Sr/^{86}Sr \cdot Sr)_{final} - (^{87}Sr/^{86}Sr \cdot Sr)_{initial} = (^{87}Sr/^{86}Sr \cdot Sr)_{plagioclase} \cdot M_{plagioclase} \tag{13}$$

The average Sr concentration of plagioclase was taken to be 344 ppm (Fiesinger et al., 1982). The plateau of isotopic values and Sr concentration between Soda Geyser and Pavilion Well (Fig. 4e) could indicate that the spring waters attain the isotopic composition of the host rock and reach fluid–mineral equilibrium by the end of the flow path. Although there is variation in the regional Sr isotopic composition of individual basalt samples (Pickett, 2004; $^{87}Sr/^{86}Sr$ values of 0.706646–0.707929, $n = 2$), the low gradient in $^{87}Sr/^{86}Sr$ towards the end of the flow path is interpreted to represent the approach to fluid–rock isotopic equilibrium (Fig. 7). On this basis the $^{87}Sr/^{86}Sr$ ratio for plagioclase used in the mass balance calculation is of the furthest down flow spring, Thunderbox spring ($^{87}Sr/^{86}Sr = 0.708508$).

The validity of the solute mass balance model can be ascertained by an alkalinity mass balance, such that the number of equivalents (mEq/l) of alkalinity produced or consumed per mole of mineral phase dissolved or precipitated must equate to the measured change in alkalinity along flow path. Giving an alkalinity mass balance model of:

$$\Delta m_{T,Alkalinity} = M_{plagioclase} + M_{pyroxene} + M_{orthoclase} + M_{gypsum} + M_{albite} + 2M_{calcite} + M_{zeolite} \tag{14}$$

where $alkalinity = [HCO_3^-] + 2[CO_3^{2-}] + [OH^-] - [H^+]$.

5.4.2. Mineral surface area

In the determination of fluid–mineral reaction kinetics the magnitude of reacting mineral surface areas is a major source of uncertainty in the calculation of dissolution rates (White and Peterson, 1990; Hellmann and Tisserand, 2006). For this study, mineral surface areas were determined geometrically and by using U-series isotopes. Geometric surface areas were calculated by assuming that fluid flow within the basalt is largely confined to open fractures, and that the exposed mineral surface area is proportional to the fracture surface area weighted for mineral volume fraction. Fracture surface areas where estimated from data in Lore et al. (2001). An independent estimate of plagioclase surface areas was made using the evolution of the U-series isotope ratio of the fluid following Andrews et al. (1982), assuming that plagioclase is the primary U hosting mineral.

5.4.2.1. U-Series-derived plagioclase surface area. The change in $^{234}U/^{238}U$ activity ratio (Fig. 8) along the flow path can be attributed to U transferred by dissolution and precipitation of U-bearing mineral phases and addition of ^{234}U due to alpha recoil from near mineral surfaces. In near surface, oxidising conditions U is most commonly in the highly soluble hexavalent U(VI) form, whereas, in reducing environment it will be in the relatively insoluble tetravalent U(IV) form (Osmond et al., 1983). The progressively more reduced nature of the CO_2-charged groundwaters at Soda Springs imply that changes in U concentrations and isotope ratios are likely to be dominated by additions from alpha recoil processes and not mineral dissolution. The evolution of $^{234}U/^{238}U$ activity ratios with time in reducing groundwater conditions was defined by Andrews et al. (1982):

$$AR_t = 1 + (AR_i - 1)\exp(-^{234}\lambda t) + 0.235\rho SR(1 - \exp(-^{234}\lambda t))(U_r/U_s) \tag{15}$$

where ρ is rock density, AR_i is the initial activity ratio of the groundwater, AR_t is the ground water activity ratio at time t, 0.235 is the fraction of the recoil atoms from within the recoil range of the surface that enter solution, R is the ^{234}Th recoil range in the rock matrix ($\approx 3 \times 10^{-6}$ cm), $^{234}\lambda$ is the ^{234}U decay constant, U_r and U_s are the U contents of the rock and groundwater respectively and S is the extent of the rock surface in contact per unit volume of ground water (m^2/m^3).

The duration of fluid–rock interaction as a function of distance along the flow path, z:

$$t = z/v = z/(0.0288\exp(-z/1646.35)k/\varphi) \tag{16}$$

where k is the bulk hydraulic conductivity (m^2) and φ is the rock porosity. The $^{234}U/^{238}U$ activity ratio of the groundwater is then expected to evolve as:

$$AR_i = 1 + (AR_i - 1)\exp(-^{234}\lambda z/(0.0288\exp(-z/1646.35)k/\varphi)) + 0.235\rho SR(1 - \exp(-^{234}\lambda z/(0.0288\exp(-z/1646.35)k/\varphi))) \times (U_r/U_s) \tag{17}$$

where ρ is the density of the fluid (m^3/kg) passing through the rock and the extent of the rock surface in contact per unit volume of ground water, S, can be related to the specific internal surface area of plagioclase, s, and the aquifer porosity, φ, by the equation (Andrews and Kay, 1983):

$$S = (\rho s)/\varphi \tag{18}$$

Substituting Eq. (18) into Eq. (17) and finding a least-squares best fit to $^{234}U/^{238}U$ versus distance (Fig. 8), the reactive surface area of plagioclase, s, was calculated to be 2.11 ± 0.35 m^2/m^3 along the entire flow path. The uncertainty reflects the scatter of data about the fit as calculated in Appendix A.

5.4.2.2. Geometric-derived plagioclase surface area. As fluid flow through the basalt aquifer is thought to be primarily along fractures, the surface area of the fractures provides an alternative estimate of fluid–mineral contact areas. The fracture data of (Lore et al., 2001) from the similar Snake River Plain basalt is used as an analogue. Specific surface areas, S ($m^2\ m^{-3}$) for plagioclase were calculated for horizontal fractures, vertical fracture and total fractures and normalised over a single basalt flow; calculated averages

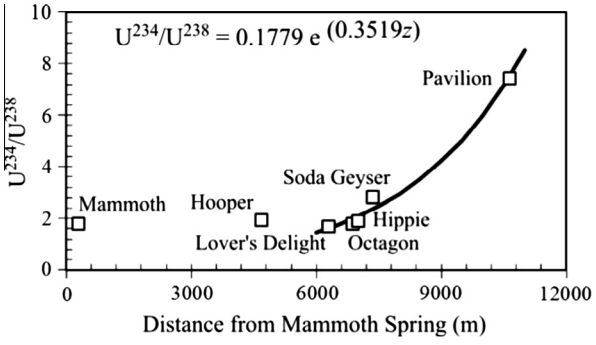

Fig. 8. Graphs of U series modelling; $^{234}U/^{238}U$ activity ratio, squares show measured values with errors less than the symbol size and the black line, fitted values.

were $1.5 \pm 1.0\ m^2\ m^{-3}$, $0.9 \pm 0.3\ m^2\ m^{-3}$ and $2.3 \pm 1.3\ m^2\ m^{-3}$, respectively. It is important to note that the horizontal and normalised plagioclase surface areas are within error of the U-series surface areas calculated earlier. As such for the reaction rate calculations only the U-series surface area will be used.

5.4.3. Reaction rates

The profile of reaction progress with distance along a flow path in a reactive-transport system is a function of the reaction rate and the rate of transport in the system (e.g. Wigley et al., 2012; Litchtner, 1992). Mineral reaction rates can therefore be calculated using the calculated gradients of mineral mole transfers in the fluid with distance along flow paths, calculated mineral surface areas and fluid flux. Plagioclase and orthoclase feldspar mineral mole transfers with distance increase at an exponentially decreasing rate downstream from Lovers Delight spring, and reaction rates were calculated from this part of the profile, where the profiles are well constrained.

A least squares fit of the change in mole transfers (M_j) with distance (z) was used to obtain the approximation (Fig. 9):

$$M_j = a \cdot \exp(z/b) + c \tag{19}$$

The rate of change of mole transfers, dM_j/dz, can then be expressed as:

$$dM_j/dz = (a \cdot exp(z/b))/b \tag{20}$$

The dissolution rate, R, for a mineral, j, is defined as:

$$R_j = (\omega_0 \varphi)/S_j \cdot (dM_j/dz) \tag{21}$$

where S_j is the mineral surface per cubic metre ($m^2\ m^{-3}$), and ω_0 ø is the fluid flux (ms^{-1}) which is calculated from the hydraulic gradient dh/dz, and the hydraulic conductivity, K (units), determined from a well discharge and recovery test, such that:

$$\omega_0 \varphi = K \cdot (dh/dz) \tag{22}$$

The rates of mineral dissolution can be calculated by a least-squares fit to the change in mineral mole transfers against distance (Eqs. (19) and (20); Fig. 8). Plagioclase dissolution rates vary from 2.4×10^{-12} to 4.6×10^{-16} mol/m^2/s and orthoclase from 2.0×10^{-13} to 6.8×10^{-16} mol/m^2/s. The difference in the reaction rate of the potassic and plagioclase feldspars is consistent with other field studies (e.g. Hereford et al., 2006; Kampman et al., 2009; White et al., 2001), but the absolute rates are several orders of magnitude slower than laboratory studies at far-from- equilibrium conditions (e.g. Brantley et al., 1993, 2007; Kim, 2002; Taylor et al., 2000; White et al., 1996; White and Brantley, 2003).

5.4.4. Approach to equilibrium

The Gibbs free energy (ΔG, kJ/mol) describes the deviation of a system from equilibrium and is defined as:

$$\Delta G = RT \cdot \ln(IAP/K_{eq}) \tag{23}$$

where R is the gas constant (kJ/K/mol), T is the absolute temperature (K), IAP is the ion activity product ($IAP_{plagioclase} = 12.26$) and K_{eq} is the equilibrium constant.

At far-from equilibrium conditions, feldspar dissolution rates are found to be approximately independent of ΔG_r (although see Taylor et al., 2000; Kampman et al., 2009). As minerals approach equilibrium with fluids numerous experimental studies have shown that reaction rates depend on the degree of mineral undersaturation. However the functional form of the reaction rate dependence on the degree of undersaturation (ΔG) is uncertain. For example Lasaga (1998) argues from transition state theory that reaction rates should exhibit a simple exponential dependence. However some experimental studies (e.g. Hellmann and

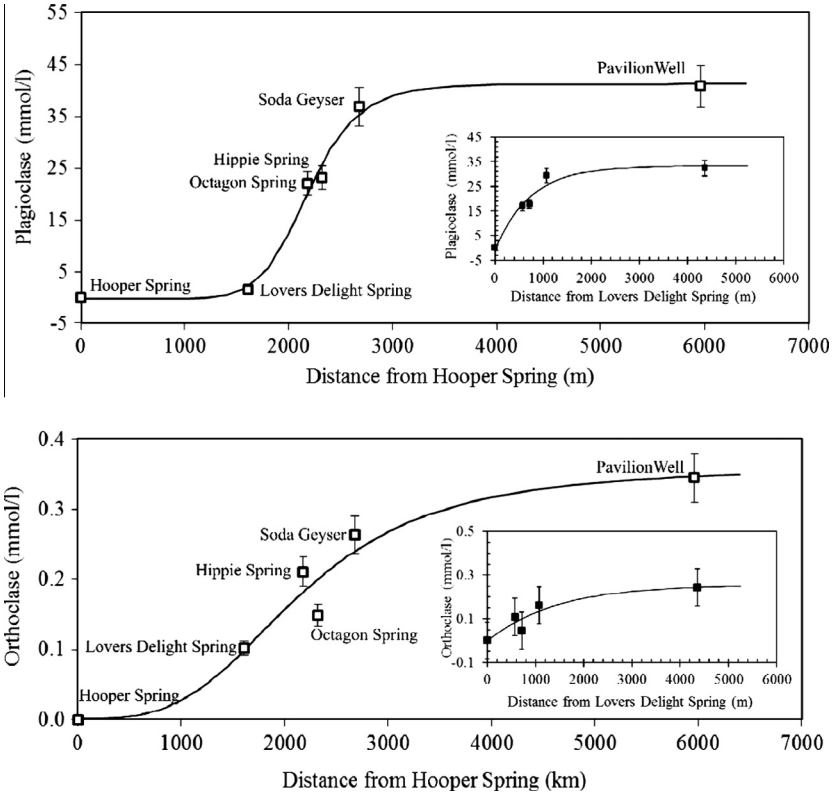

Fig. 9. Calculated changes in mole transfers of feldspar with distance along flow path. The rate of change of mineral moles with distance was calculated by a least-squares fit to Eq. (19). Error bars are the propagated uncertainty associated with mass balance modelling (Appendix A and B).

Tisserand, 2006) and field studies (e.g. Kampman et al., 2009) imply a different function form with the gradient of reaction rate change decreasing as equilibrium is approached.

The degree of disequilibrium between fluids and minerals in this study has been calculated by using the activities and equilibrium constants of aqueous species from the geochemical computer code PHREEQC (Parkhurst and Appelo, 1999). As pH and alkalinity were measured at surface, the total CO_2 concentration is underestimated due to surface degassing. Therefore ΔG was calculated assuming CO_2 was saturated at the depth sampled by the spring and this depth was estimated from the local geothermal gradient and spring temperatures. Values for ΔG for plagioclase ($\Delta G_{plagioclase}$) were determined using Eq. (23), where a K_{eq} value was calculated using SUPCRT92, using a plagioclase solid solution composition of $Ca_{0.5}Na_{0.5}AlSi_3O_8$. As fluids are oversaturated in respect to orthoclase we did not calculate ΔG values for R_{kspar}. Fig. 10 displays an inverse relationship between dissolution rates and mineral–fluid free energies over a −25.4 to −10.8 kJ/mol transition. The proximity of these free energies to equilibrium lie in the moderate to low ΔG, low dissolution rate range, characterised by a strong functional dependence of the dissolution rate on ΔG. At $\Delta G_{plagioclase} > -30$ kJ/mol rates decrease exponentially over four orders of magnitude as equilibrium is approached thus accounting for the large range in calculated reaction rates.

These observations support other field studies (e.g. Maher, 2010; Maher et al., 2009; Malmstrom et al., 2000; Kampman et al., 2009) that natural mineral weathering rates occur largely in the close to equilibrium region difficult to characterise in laboratory experimental studies (c.f. Hellmann and Tisserand, 2006).

5.4.5. Uncertainties

The uncertainties in calculated reaction rates result from uncertainties in fluid residence times, hydraulic conductivity, hydraulic gradients, flow paths, surface areas, secondary mineral compositions and past variations in isotopic compositions of groundwater. Estimating reactive mineral surface areas is one of the most problematic aspects of determining mineral reaction rates (White and Brantley, 2003). Reactive mineral surface areas are assumed to be constant along the length of the flow path. Errors for the hydraulic gradient are assumed to be on the order of ±10%. Errors were propagated for calculations of mole transfers and reaction rate using the equations in Appendices A and B. It should noted that several of these factors, including most significantly the estimates of mineral surface areas, are probably systematic and although affecting the absolute mineral dissolutions rates, will not change the relationship between reaction rate and degree of undersaturation.

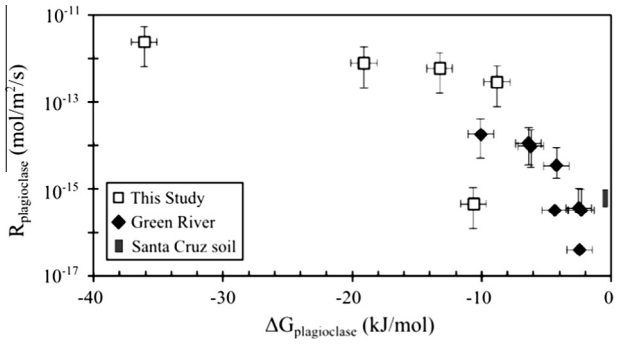

Fig. 10. Variations in plagioclase dissolution rate with respect to ΔG from a compilation of in-situ dissolution rates showing the strong dependence of reaction rates on the degree of under-saturation. Compiled data from Green River (Kampman et al., 2009), Santa Cruz soil (Maher et al., 2009) and this study. Error bars for $R_{plagioclase}$ in this study are propagated using the equations detailed in Appendix B.

6. Conclusion

Establishing reliable rates for low-temperature silicate dissolution and precipitation reactions is critical to the understating of fluid–mineral reaction rates in storage reservoirs and the long-term security of the stored CO_2. Understanding processes controlling the absolute magnitude of these rates, including mineral surface, thermodynamic and fluid transport process, is important for informing modelling studies. This study uses the chemical evolution of groundwater from the lower CO_2-charged aquifer in the Blackfoot Lava Field to examine the fluid–mineral reactions occurring within a basaltic aquifer. Groundwater flow is confined to open fractures within the basalt. North–northwest trending faults allowing the vertical migration of waters to the surface resulting in the occurrence of CO_2-rich springs. An in-situ bulk hydraulic conductivity of $1.2 \times 10^{-4} \pm 1.1 \times 10^{-4}$ m/min was determined using pressure recovery data from a flowing well penetrating the CO_2-charged portion of the aquifer. Interpolated potentiometric surfaces, determined from hydraulic head data, were used to determine regional flow paths between the CO_2-springs. The initial composition of meteorically-derived groundwater is sourced from the northern recharge zone, Blackfoot Reservoir. Solute concentrations increase along flow paths due to CO_2-promoted weathering of minerals comprising the aquifer matrix. Changes in groundwater chemistry and petrological observations, are used to infer that these reactions are dominated by feldspar dissolution and zeolite precipitation. Increases in pH and HCO_3^- along the flow path indicate that the fluid–mineral reactions are dominated by the hydrolysis of silicate minerals consuming H^+ and releasing alkalinity.

In-situ feldspar dissolution rates were determined from mass balance modelling of fluid chemistry along the flow path from Lovers Delight Spring down-gradient and constrained by petrology, whole rock chemistry and aquifer hydrology. Calculated plagioclase dissolution rates range from 4.6×10^{-12} to 4.6×10^{-16} mol/m^2/s and orthoclase feldspar dissolution rates from 2.0×10^{-13} to 6.8×10^{-16} mol/m^2/s. These rates are one to four orders of magnitude slower than rates determined by laboratory experiments at similar pH and temperatures. It is interesting to note that the dissolution rates of plagioclase are an order of magnitude faster than orthoclase, which is consistent with findings of White et al. (2001), Hereford et al. (2006) and Kampman et al. (2009). ΔG values of plagioclase indicate near-equilibrium conditions of waters with reaction rates decreasing sharply with increasing saturation; indicating a strong functional dependence of reaction kinetics on the free energy of fluid–mineral reactions. These findings are in agreement with similar studies of near-equilibrium silicate dissolution both in flow through laboratory reactor experiments (Hellmann et al., 2007); and natural analogue sites such as at Green River, Utah (Kampman et al., 2009). Major uncertainties in this study, as is common in most field studies, originate from the non-unique interpretations of mass balance modelling, the difficulty of defining and measuring reactive surface areas, the heterogeneities in mineral compositions and groundwater chemistry over the flow path.

Acknowledgements

Max Wigley and Benoit Dubacq are thanked for their helpful discussions. Carbon research at Cambridge is supported by Natural Environment Research Council grant NE/F004699/1, part of the UK CRIUS (Carbon Research Into Underground Storage) consortium and DECC through the '£20 million' competition. Niko Kampman acknowledges financial support from Shell Global Solutions International.

Appendix A. Uncertainties on fitted parameters

Parameters are fitted by minimising the goodness of fit parameter chi-squared, defined as:

$$\chi^2 = \sum((\psi_{calc} - \psi_{obs})/\sigma_\psi) \quad (A.1)$$

(e.g. Bevington and Robinson, 2003) where ψ_{calc} and ψ_{obs} are the modelled and observed data at distance along flow path and σ_ψ is the error associated with the analyses. The uncertainties associated with fitted parameters have then been estimated using a Monte Carlo simulation. Uncertainties have been estimated with the requirement that the chi-squared value (χ^2; Eq. (A.1)) for the fit of the model to the data is appropriate for the number of degrees of freedom. The fit of the model to the data is thought to be adequate when the value of χ^2/ν (defining the reduced χ^2, where ν is the number of degrees of freedom) is one. In the present case the analytical uncertainty of the data is much smaller than the misfit of the model to the data. For example for the fits presented in Fig. 8 obtained values for χ^2/ν are in the range from 9 to 28. The best fit of the model has then been re-evaluated 500 times within a Monte-Carlo simulation with each data point varying randomly within its uncertainty. Using the maximum uncertainties allows the Monte-Carlo simulation to provide a greater, more realistic estimation of errors on the calculated reaction rates. The obtained distribution is centred over the best-fit value and its uncertainty may be evaluated from the spread around the mean.

Appendix B. Error propagation

Uncertainties for the modelled mineral mass transfers were determined by using the Gaussian error propagation method (Barrante, 1974), from the elemental uncertainties of analytically determined parameters and the uncertainties of all modelled components. We use the linear propagation method of Anderson (1976) to calculate the uncertainty by treating the mass balance equations as a set of dependent linear equations.

$$\sigma^2_{M_{Kspar}} = \{\sigma_K\}^2_{final} + \{\sigma_K\}^2_{initial} \quad (B.1)$$

$$\sigma^2_{M_{Plag}} = \left\{\frac{\sigma_{^{87}Sr/^{86}Sr}}{^{87}Sr/^{86}Sr}\right\}^2_{final} + \left\{\frac{\sigma_{Sr}}{Sr}\right\}^2_{final} + \left\{\frac{\sigma_{^{87}Sr/^{86}Sr}}{^{87}Sr/^{86}Sr}\right\}^2_{initial} + \left\{\frac{\sigma_{Sr}}{Sr}\right\}^2_{initial} + \left\{\frac{\sigma_{^{87}Sr/^{86}Sr}}{^{87}Sr/^{86}Sr}\right\}^2_{plag} + \left\{\frac{\sigma_{Sr}}{Sr}\right\}^2_{plag} \quad (B.2)$$

The uncertainty in calculated reaction rates can be defined as:

$$\sigma R_j^2 = \left\{\left(\frac{M_j\omega_0}{S_j}\right)\sigma\varphi\right\}^2 + \left\{\left(\frac{M_j\omega_0\varphi}{S_j^2}\right)\sigma S_j\right\}^2 + \left\{\left(\frac{\omega_0\varphi}{S_j}\right)\sigma M_j\right\}^2 + \left\{\left(\frac{M_j\varphi}{S_j}\right)\sigma\omega_0\right\}^2 \quad (B.3)$$

Appendix C. Supplementary material

Supplementary data associated with this article can be found, in the online version, at http://dx.doi.org/10.1016/j.apgeochem.2015.06.010.

References

Allmendinger, R.W., 1981. Structural geometry of Meade thrust plate in Northern Blackfoot Mountains Southeastern Idaho. AAPG Bull., 65

Allmendinger, R.W., Jordan, T.E., 1981. Mesozoic evolution, hinterland of Sevier orogenic belt. Geology 9, 308–313.

Anderson, G.M., 1976. Error propagation by the Monte Carlo method in geochemical calculations. Geochim. Cosmochim. Acta 40, 1533–1538.

Andrews, J.N., Giles, I.S., Kay, R.L.F., Lee, D.J., Osmond, J.K., Cowart, J.B., Fritz, P., Barker, J.F., Gale, J., 1982. Radioelements, radiogenic helium and age relationships for groundwaters from the granites at Stripa, Sweden. Geochim. Cosmochim. Acta 46, 1533–1543.

Andrews, J.N., Kay, R.L.F., 1983. $^{234}U/^{238}U$ activity ratios of dissolved uranium in groundwaters from a Jurassic limestone aquifer in England. Earth Planet. Sci. Lett. 57, 139–151.

Armstrong, F., Leeman, W.P., Malde, H.E., 1975. K-Ar dating, Quaternary and Neogene volcanic rocks of the Snake River Plain, Idaho. Am. J. Sci. 275, 225–251.

Armstrong, F., Oriel, S., 1965. Tectonic development of Idaho-Wyoming Thrust Belt. Am. Assoc. Pet. Geol. Bull. 49, 1847–1866.

Barrante, J.R., 1974. Applied Mathematics for Physical Chemistry. Prentice-Hall, Englewood Cliffs, New Jersey.

Benjamin, L., Knobel, L.L., Hall, L.F., Cecil, L.D., Green, J.R., 2004. Development of a Local Meteoric Water Line for Southeastern Idaho, Western Wyoming, and South-Central Montana. Scientific Investigations Report 2004-5126. U.S. Geological Society, Idaho Falls, Idaho.

Bevington, P.R., Robinson, D.K., 2003. Data Reduction and Error Analysis for the Physical Sciences. McGraw-Hill Higher Education, McGraw-Hill, 137.

Bickle, M.J., Bunbury, J., Chapman, H.J., Harris, N.B.W., Fairchild, I.J., Ahmad, T., 2003. Fluxes of Sr into the headwaters of the Ganges. Geochim. Cosmochim. Acta 67, 2567–2584.

Bickle, M.J., Bunbury, J., Chapman, H.J., Harris, N.B.W., Fairchild, I.J., Ahmad, T., Pomies, C., 2005. Relative contributions of silicate and carbonate rocks to riverine Sr fluxes in the headwaters of the Ganges. Geochim. Cosmochim. Acta 69, 2221–2240.

Bisroy, Y.K., Summers, W.K., 1980. Determination of aquifer parameters from step tests and intermittent pumping data. Ground Water 18 (2), 137–146.

Brantley, S., Blai, A., Cremeens, D., Macinnis, I., Darmody, R., 1993. Natural etching rates of feldspar and hornblende. Aquat. Sci.-Res. Across Bound. 55, 262–272.

Brantley, S., Kubicki, J., White, A., 2007. Kinetics of Water–Rock Interaction. Springer Verlag, New York.

Bright, J., Kaufman, D.S., Forester, R.M., Dean, W.E., 2006. A continuous 250,000 yr record of oxygen and carbon isotopes in ostracode and bulk-sediment carbonate from Bear Lake, Utah-Idaho. Quatern. Sci. Rev. 25, 2258–2270.

Burchfiel, C., Cowan, D.S., Davis, G.D., 1992. Tectonic overview of the Cordilleran orogen in the western United States. In: Burchfiel, C., Lipman, P.W., Zoback, M.L. (Eds.), The Cordilleran Orogen: Conterminous. The Geological Society of America, U.S. Boulder, Colorado.

Camilleri, P.A., Yonkee, A., Coogan, J., Decelles, P.G., Mcgrew, A., Wells, M.L., 1997. Hinterland to foreland transect through the Sevier Orogen, northeast Nevada to north central Utah: structural style, metamorphism, and kinematic history of a large contractional orogenic wedge. In: Link, P.K., Kowallis, B. (Eds.), Geological Society of America Fieldtrip Guide for the 1997 National Meeting. Brigham Young University Geology Studies.

Drever, J.I., 1988. The Geochemistry of Natural Waters, second ed. Prentice Hall Inc, Englewood Cliffs, New Jersey, 402p.

Fiesinger, D.W., Perkins, W.D., Puchy, B.J., 1982. Mineralogy and petrology of Tertiary–Quaternary volcanic rocks in Caribou County, Idaho. In: Bonnichsen, B., Breckenridge, R.M. (Eds.), Cenozoic Geology of Idaho. Idaho Geological Survey Bulletin, Moscow, Idaho.

Graham, W.G., Campbell, L.J., 1981. Groundwater Resources of Idaho, Water. Boise.

Hellmann, R., Daval, D., Tisserand, D., Renard, F., 2007. Albite feldspar dissolution kinetics as a function of the Gibbs free energy at high pCO_2. In: Bullen, T.D., Wang, Y. (Eds.), Water–Rock Interaction. Taylor and Francis.

Hellmann, R., Tisserand, D., 2006. Dissolution kinetics as a function of the Gibbs free energy of reaction: an experimental study based on albite feldspar. Geochim. Cosmochim. Acta 70, 364–383.

Hereford, A.G., Keating, E.H., Guthrie, G.D.J., Zhu, C., 2006. Reactions and reaction rates in the regional aquifer beneath the Pajarito Plateau, north-central New Mexico, USA. Environ. Geol. 52, 965–977.

Hutsinpiller, A., Parry, W., 1985. Geochemistry and geothermometry of spring water from the Blackfoot Reservoir region, southeastern Idaho. J. Volcanol. Geoth. Res. 26, 275–296.

Idaho Department of Water Resources, 2012. Well Driller Reports (Logs). <http://www.idwr.idaho.gov/WaterManagement/WellInformation/DrillerReports/dr_default.htm> (accessed 29.08.12).

Intergovernmental Panel on Climate Change, 2013. The Physical Science Basis. Contribution of Working Group I to the Fifth Assessment Report of the Intergovernmental Panel on Climate Change. Cambridge University Press, Cambridge, United Kingdom and New York, NY, USA.

Janecke, S.U., Evans, J.C., 1999. Folded and faulted Salt Lake Formation above the Miocene to Pliocene(?) New Canyon and Clifton detachment faults, Malad and Bannock ranges, Idaho: field trip guide to the Deep Creek half graben and environs. In: Hughes, S.S., Thackray, G.D. (Eds.), Guidebook to the Geology of Eastern Idaho. Idaho Museum of Natural History, Pocatello, Idaho.

Jeandel, E., Battani, A., Sarda, P., 2010. Lessons learned from natural and industrial analogues for storage of carbon dioxide. Int. J. Greenhouse Gas Control 4, 890–909.

Jiménez-Moreno, G., Scott Anderson, R., Fawcett, P.J., 2007. Orbital- and millennial-scale vegetation and climate changes of the past 225 ka from Bear Lake, Utah, Idaho (USA). Quat. Sci. Rev. 26, 1713–1724.

Johnson, J., Anderson, G., Parkhurst, D.L., 2000. Database 'thermo.com.V8.R6.230', Rev. 1.11. Lawrence Livermore National Laboratory, Livermore, California.

Kampman, N., Bickle, M., Becker, J., Assayag, N., Chapman, H., 2009. Feldspar dissolution kinetics and Gibbs free energy dependence in a CO_2-enriched groundwater system, Green River, Utah. Earth Planet. Sci. Lett. 284, 473–488.

Kelemen, P.B., Matter, J.M., 2008. In situ carbonation of peridotite for CO_2 storage. Proc. Natl. Acad. Sci. USA 105, 295–300.

Kelemen, P.B., Matter, J.M., Streit, E.E., Rudge, J.F., Curry, W.B., Blusztajn, J., 2011. Rates and mechanisms of mineral carbonation in peridotite: natural processes and recipes for enhanced in situ CO_2 capture and storage. Proc. Natl. Acad. Sci. USA 39, 545–576.

Kim, K., 2002. Plagioclase weathering in the groundwater system of a sandy, silicate aquifer. Hydrol. Process. 16, 1793–1806.

Lasaga, A.C., 1998. Kinetic Theory in the Earth Sciences. Princeton University Press, Princeton, New-Jersey.

Lewicki, J.L., Hilley, G.E., Dobeck, L., McLing, T.L., Kennedy, B.M., Bill, M., Marino, B.D.V., 2013. Geologic CO_2 input into groundwater and the atmosphere, Soda Springs, ID, USA. Chem. Geol. 339, 61–70.

Litchner, P.C., 1992. Time space continuum description of fluid–rock interaction in permeable media. Water Resour. Res. 28, 3135–3155.

Lore, J., Aydin, A., Goodson, K., 2001. A deterministic methodology for prediction of fracture distribution in basaltic multiflows. J. Geophys. Res. 106, 6447–6459.

Luo, S., Ku, T.-L., Roback, R., Murrell, M., McLing, T.L., 2000. In-situ radionuclide transport and preferential groundwater flows at INEEL (Idaho): decay-series disequilibrium studies. Geochim. Cosmochim. Acta 64, 867–881.

Mabey, D., Oriel, S., 1970. Gravity and Magnetic Anomalies in the Soda Springs Region, Southeastern Idaho. U.S. Geological Survey Professional Paper.

Maher, K., 2010. The dependence of chemical weathering rates on fluid residence time. Earth Planet. Sci. Lett. 294 (1–2), 101–110. http://dx.doi.org/10.1016/j.epsl.2010.03.010.

Maher, K., DePaolo, D.J., Lin, J.C.-F., 2004. Rates of silicate dissolution in deep-sea sediment; in situ measurement using $^{234}U/^{238}U$ of pore fluids. Geochim. Cosmochim. Acta 68 (22), 4629–4648. http://dx.doi.org/10.1016/j.gca.2004.04.024.

Maher, K., Steefel, C.I., White, A.F., Stonestrom, D.A., 2009. The role of reaction affinity and secondary minerals in regulating chemical weathering rates at the Santa Cruz soil chronosequence, California. Geochim. Cosmochim. Acta 73 (10), 2804–2831. http://dx.doi.org/10.1016/j.gca.2009.01.030.

Malmstrom, M.E., Destouni, G., Banwart, S.A., Stromberg, B.H.E., 2000. Resolving the scale-dependence of mineral weathering rates. Environ. Sci. Technol. 34, 1375–1378.

Martínez-Aguirre, A., Morón, M., García-León, M., 1991. Measurements of U- and Ra-isotopes in rainwater samples. J. Radioanal. Nucl. Chem. 152, 37–46.

Matter, J.M., Kelemen, P.B., 2009. Permanent CO_2 storage and mineral carbonation in geologic reservoirs. Nat. Geosci. 2, 837–841.

Miller, D.M., 1991. Mesozoic and Cenozoic tectonic evolution of the northeastern Great Basin. In: Buff, R.H., Coyner, A.R. (Eds.), Geology and Ore Deposits of the Great Basin: Field Trip Guidebook Compendium. Geological Society of Nevada.

Mitchell, J., 1976. Geothermal Investigations in Idaho: Part 6. Idaho Department of Water Resources Bulletin.

Oriel, S., 1968. Preliminary Geologic Map of Bancroft (15-min) Quadrangle, Caribou and Bannock Counties, Idaho. U.S. Geological Survey Open-File Map, 68-204.

Oriel, S., Platt, L.B., 1980. Geological Map of the Preston 1×2 min Quadrangle, Southeastern Idaho and Western Wyoming. U.S. Geological Survey Miscellaneous Geological Investigations Map, I-1127.

Osmond, J.K., Cowart, J.B., 1976. The theory and uses of natural uranium isotopic variations in hydrology. Atom. Energy Rev. 14, 621–679.

Osmond, J.K., Cowart, J.B., Ivanovich, M., 1983. Uranium isotopic disequilibrium in ground water as an indicator of anomalies. Int. J. Appl. Radiat. Isotop. 34, 283–308.

Parkhurst, D.L., Appelo, C.A.J., 1999. User's Guide to PHREEQC (version 2) – A Computer Program for Speciation, Batch Reaction, One Dimensional Transport, and Inverse Geochemical Calculations. U.S. Geological Survey Water-Resources Investigations Report, 99, 312.

Pickett, K.E., 2004. Physical Volcanology, Petrography, and Geochemistry of Basalts in the Bimodal Blackfoot Volcanic Field, Southeastern Idaho. Department of Geosciences. Boise, Idaho State University.

Ralston, D.R., Arrigo, J., Baglio, J.J., Coleman, L., Hubbell, J., Souder, K., Mayo, A.L., 1983. Thermal Ground Water Flow Systems in the Thrust Zone in Southeastern Idaho. Idaho Department of Water Resources Technical Report, 336.

Roback, R.C., Johnson, T.M., McLing, T.L., Murrell, M.T., Luo, S., Ku, T.-L., 2001. Uranium isotopic evidence for groundwater chemical evolution and flow patterns in the eastern Snake River Plain aquifer, Idaho. Geol. Soc. Am. Bull. 113, 1133–1141.

Sacks, P.E., Platt, L.B., 1985. Depth and timing of decollement extension, southern Portneuf range, southeastern Idaho. In: Kerns, G.J., Kerns, R.L.J. (Eds.), Orogenic Patterns and Stratigraphy of North-Central Utah and Southeastern Idaho. Utah Geological Association Publication.

Stumm, W., Morgan, J.J., 1996. Aquatic Chemistry, Chemical Equilibria and Rates in Natural Waters. John Wiley & Sons Inc., New York.

Taylor, A.S., Blum, J.D., Lasaga, A.C., 2000. The dependence of labradorite dissolution and Sr isotope release rates on solution saturation state. Geochim. Cosmochim. Acta 64, 2389–2400.

U.S. Army Corps of Engineers, 1968. Hydrology, Blackfoot Dam and Reservoir, Blackfoot River, Idaho. Design Memoir, 1.

White, W.M., 2011. Trace Elements in Igneous Processes. Geochemistry. Cornell University, New York (Chapter 7).

White, A.F., Blum, A., Schulz, M., Bullen, T., Harden, J., Peterson, M., 1996. Chemical weathering rates of a soil chronosequence on granitic alluvium: I. Quantification of mineralogical and surface area changes and calculation of primary silicate reaction rates. Geochim. Cosmochim. Acta 60, 2533–2550.

White, A.F., Brantley, S.L., 2003. The effect of time on the weathering of silicate minerals: why do weathering rates differ in the laboratory and field? Chem. Geol. 202, 479–506.

White, A.F., Bullen, T.D., Schulz, M.S., Blum, A.E., Huntington, T.G., Peters, N.E., 2001. Differential rates of feldspar weathering in granitic regoliths. Geochim. Cosmochim. Acta 65, 847–869.

White, A.F., Peterson, M.L., 1990. Role of Reactive-Surface-Area Characterization in Geochemical Kinetic Models. Chemical Modeling of Aqueous Systems II. American Chemical Society.

Wigley, M., Kampman, N., Dubacq, B., Bickle, M., 2012. Fluid–mineral reactions and trace metal mobilization in an exhumed natural CO_2 reservoir, Green River, Utah. Geology 40, 555–558.